Dual-Modal MRI Contrast Agent with Aggregation-Induced Emission Characteristic for Liver Specific Imaging with Long Circulation Lifetime

Yilong Chen,[†,‡,⊥] Min Li,[§,⊥] Yuning Hong,[‡] Jacky W. Y. Lam,[‡] Qichang Zheng,*[§] and Ben Zhong Tang*[†,‡,∥]

[†]HKUST Shenzhen Research Institute, No. 9 Yuexing 1st RD, South Area, Hi-tech Park Nanshan, Shenzhen 518057, China

[‡]Department of Chemistry, Institute for Advanced Study, Division of Biomedical Engineering, Division of Life Science, Institute of Molecular Functional Materials and State Key Laboratory of Molecular Neuroscience, The Hong Kong University of Science & Technology (HKUST), Clear Water Bay, Kowloon, Hong Kong, China

[§]Department of Hepatobiliary Surgery, Union Hospital, Tongji Medical College, Huazhong University of Science and Technology, Wuhan 430022, China

[∥]Guangdong Innovative Research Team, SCUT-HKUST Joint Research Laboratory, State Key Laboratory of Luminescent Materials and Devices, South China University of Technology (SCUT), Guangzhou 510640, China

Ⓢ Supporting Information

ABSTRACT: We herein report a novel dual-modal MRI contrast agent, TPE-2Gd, for both magnetic and fluorescence imaging. TPE-2Gd consists of a hydrophobic tetraphenylethene (TPE) fluorophore and two hydrophilic gadolinium (Gd) diethylenetriaminepentaacetic acid moieties. As an amphiphilic molecule, TPE-2Gd aggregates into micelles at a high concentration in aqueous medium. These aggregates are highly emissive, showing an aggregation-induced emission (AIE) characteristic. TPE-2Gd is used as a fluorescent agent for cell imaging, which demonstrates negligible cytotoxicity and excellent photostability owing to its AIE property. As a magnetic resonance imaging (MRI) contrast agent, TPE-2Gd exhibits similar longitudinal relaxivity in water ($R_{1,TPE-2Gd}$ = 3.36 ± 0.10 s^{-1} per mM of Gd^{3+}) as those commercial agents (e.g., Magnevist, $R_{1,magnevist}$ = 3.70 ± 0.02 s^{-1} per mM of Gd^{3+}). Compared with Magnevist, the circulation lifetime of TPE-2Gd nanoaggregates in living rats is extended from 10 min to 1 h. With relatively high specificity to the liver, the MR imaging could remain hyperintense in liver even after 150 min post injection. These TPE-2Gd nanoparticles can be excreted gradually via renal filtration due to the disassembly of the nanoparticles into small molecules during circulation. TPE-2Gd could thus potentially be used as a liver specific MRI contrast agent for clinical diagnosis.

KEYWORDS: aggregation-induced emission, long circulation lifetime, dual-modal MRI contrast agent, teraphenylethene derivatives, cell imaging

TPE-2Gd

T_1-weighted MR images of rat liver

Baseline   150 min
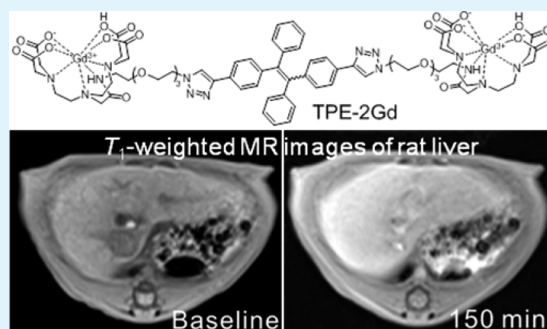
1. INTRODUCTION

The magnetic resonance imaging (MRI) technique is a noninvasive tool that has been widely used in clinical diagnosis in the past three decades.[1] This is because MRI is free of penetration depth limitation and radiation harm, which are the biggest obstacles of using optical and computed tomography methods, respectively. Globally, there are more than 60 million diagnostic MRI scans carried out per year;[2] the MRI contrast agent market was worth 1.1 billion U.S. dollars in 2010. The most commonly used MRI contrast agents are based on paramagnetic metal ion chelates with unpaired electrons, which can decrease the T_1 and T_2 relaxation time of the nearby spins. Gadolinium (Gd) chelates are representative T_1 contrast agents that can effectively decrease T_1. All clinically approved Gd contrast agents are small molecules. Small molecules with size less than 5 nm, however, can easily pass through the renal pores and be eliminated via the rapid blood pool clearance by the kidney. Short circulation lifetime in blood intrinsically limits the improvement of image resolution.[3] Alternatively, macromolecular and nanostructured MRI contrast agents, such as polymers, dendrimers, and supramolecular-based self-assembled structures, are attracting increasing attention in recent years.[4−8] These contrast agents, with large size, could improve the pharmacokinetics and allow the application of more high-resolution imaging techniques and modalities to enhance the resolution and accuracy for early stage diagnosis. Furthermore, macromolecular

and nanostructured contrast agents possess enhanced permeability and retention (EPR) effects on solid tumors due to the increased leaky vasculature associated with fast-growing malignancies,[9] showing improved specificity to the tumors. However, despite the poor reproducibility, the macromolecular MRI contrast agents are excreted with difficulty after administration, posing potential chronic toxicity. Because of this concern, few macromolecular contrast agents are commercialized. Ideally, a MRI contrast agent with a circulation lifetime long enough for high resolution imaging and short enough for body clearance is desirable. Self-assembled or aggregated nanostructures of small molecular MRI contrast agents may fulfill these requirements. Their nanoscaled size could enhance the blood pool retention and thus the circulation lifetime; the self-assembled nanoaggregates could be gradually disassembled and eliminated thoroughly after administration.[4−8]

On the other hand, optical techniques especially fluorescence microscope provides better visibility and higher resolution, while fluorescent microscope is limited for depth problem. Materials which can provide both MRI and fluorescence signals would be perfect imaging agents providing high resolution and no depth limitation.[10−12] The first MRI-fluorescent dual-modal probes were reported by Meade et al. in 1998, which contain both a Gd chelator and a fluorophore tetramethylrhodamine.[13] Although the agent exhibited both MRI and fluorescence signals in vitro, only fluorescence signals were detectable in vivo in *Xenopus laevis* embryos. This was explained by the accumulation of the molecules in fatty tissues where little or no water exchange can take place, as a result, no MRI signals. Later on, most multimodal MRI contrast agents reported are based on the modification of polymers; the molecular design for small molecule multimodal MRI contrast agent is rare and less reported.[14,15]

Our group has discovered a novel aggregation-induced emission (AIE) phenomenon on a series of propeller shaped molecules. These molecules are nonemissive in solution and highly fluorescent upon aggregate formation, which is contradicted to the expected aggregation caused quench (ACQ) effect of most traditional fluorophores.[16] Restriction of intramolecular rotation was proposed as the main cause of the AIE effect.[17,18] Fluoregens bearing the AIE characteristic have been widely explored in OLED, sensing, and bioimaging applications.[17−19] Tetraphenylethene (TPE) is one of the most famous AIE fluorogens because of its high emission efficiency and accessible synthesis. To achieve the dual functionalities, in this work, we synthesized a TPE derivative containing Gd-diethylenetriamine pentaacetic acid (DTPA) chelates (TPE-2Gd). The utilization of TPE-2Gd for cell imaging was examined and the feasibility of using TPE-2Gd as a MRI contrast agent was demonstrated. Because of the formation of nanoaggregate, TPE-2Gd displays prolonged blood circulation lifetime and thus enhance MRI resolution and biodistribution in live rats.

2. EXPERIMENTAL SECTION

2.1. Materials. 1,2-Bis(4-ethynylphenyl)-1,2-diphenylethene (**1**) and 2-(2-(2-(2-azidoethoxy)ethoxy)ethoxy)ethanamine (**2**) were synthesized according to the methods provided in the literature.[20,21] Copper(I) bromide, pentamethyldiethylenetriamine (PMDETA), dicyclohexyl-carbodiimide (DCC), 4-(dimethylamino) pyridine (DMAP), triethylamine, diethylenetriamine pentaacetic dianhydride (**4**), gadolinium(III) acetate hydrate, sodium acetate, trifluoroacetic acid, and other chemicals and solvents (Analytical grade) were all purchased from Aldrich and used as received without further purification. Distilled water was used throughout the experiments. Human cervical cancer HeLa cells were obtained from the American

Type Culture Collection (ATCC; Rockville, MD). Culture medium and fetal bovine serum were purchased from Gibco Laboratories (Grand Island, NY). 3-(4,5-Dimethylthiazol-2-yl)-2,5-diphenyltetrazolium bromide (MTT) and propidium iodide (PI) were purchased from Sigma. Commercial contrast agent Magnevist was purchased from Schering AG (Berlin, Germany). Male Sprague−Dawley (SD) rats were purchased from the Center of Experimental Animals (Tongji Medical College, Huazhong University of Science and Technology).

2.2. Instruments. ^{1}H and ^{13}C NMR spectra were measured on Bruker ARX 400 NMR spectrometers using DMSO-d_6 or D_2O as the deuterated solvent with TMS as the internal standard. IR spectra were recorded on a Bruker spectrophotometer (Tensor 27). High-resolution mass spectra (HRMS) were recorded on a Finnigan MAT TSQ 7000 mass spectrometer system operating in MALDI-TOF mode. Melting points (mp) were measured on an electrothermal digital melting point apparatus (Barnstead Electrothermal, 9100). X-ray photoelectron spectroscopy (XPS) experiments were carried out for the elemental composition analysis of TPE-2Gd on surface analysis Kratos Axis Ultra system (Axis Ultra DLD) with Al Kα radiation (hv = 1486.6 eV) operated at 150 W calibrated using the peak of adventitious carbon (C 1s peak at 285.0 eV). Wide scan spectra were recorded at a resolution pass energy of 160 eV and elemental peaks at a resolution pass energy of 40 eV. UV−vis absorption spectra were recorded on a Cary 50 Conc UV−visible spectrometer. Photoluminescence (PL) spectra were recorded on a PerkinElmer spectrofluorometer LS 55. The quantum yield value of solid powder was determined using an integrating sphere method. Particle sizes were measured on a zeta potential analyzer (Brookhaven, ZETAPLUS). The morphology of TPE-2Gd aggregates was investigated using transmission electron microscopy (TEM; Japan, JEOL JEM 100CXII) at an accelerating voltage of 100 kV. For cell imaging experiments, HeLa cells were imaged under a LSM7 DUO confocal laser scanning microscope (CLSM; Carl Zeiss, Germany). For cytotoxicity experiments, cells were treated with MTT and the absorbance was measured on a 1420 Victor Multi-Label Counter (PerkinElmer Life Science). The in vitro and in vivo MRI imaging was carried out on 3.0 T Siemens Tim Trio MRI scanner (Siemens Medical Solutions, Erlangen, Germany) equipped with a human head coil.

2.3. Synthesis. 3 was synthesized via click reaction with the feed ratio of reagents [**1**]/[**2**]/[CuBr]/[PMDETA] (1:2.2:2.2:2.2). **1** (380.5 mg, 1 mmol) and **2** (479.9 mg, 2.2 mmol) were added to a 50 mL Schlenk flask and dissolved in 30 mL of dimethylformamide (DMF). CuBr (315.6 mg, 2.2 mmol) and PMDETA (9.72 mL, 2.2 mmol, diluted by 10 mL DMF) were then added as catalysts. The reaction was conducted at 35 °C for 36 h. Then the reaction mixtures were diluted with water (300 mL) and the aqueous solution was extracted with dichloromethane (DCM) four times. The combined organic phases were further washed with brine six times and dried over Na_2SO_4. After solvent evaporation, the resulting residue was dissolved in 30 mL of DCM and then precipitated in ethyl ether three times to give the corresponding desired yellow solid compound **3** in 64% yield (mp 65.3 ± 1.4 °C). ^{1}H NMR (400 MHz, DMSO-d_6, δ): 8.41 (m, 2H, H of triazole), 7.60 (m, 4H; H−Ar−triazole), 7.12−7.01 (m, 14H; H−Ar), 4.51 (s, 4H; CH_2−triazole), 3.81 (m, 4H; CH_2C−triazole), 3.54−3.13 (m, 24H; OCH_2 and NCH_2); ^{13}C NMR (100 MHz, DMSO-d_6, δ): 145.9, 143.0, 142.6, 140.4, 131.3, 130.7, 129.0, 127.9, 126.7, 124.6, 121.8, 69.6, 68.6, 49.6; IR (KBr): ν = 3440.9, 2868.1, 1647.2, 1492.9, 1454.3, 1352.1, 1294.2, 1253.7, 1226.7, 1109.1, 972.1, 927.8, 844.8, 813.9, 761.9, 700.2, 628.8, 596.0, 572.9 cm^{-1}; HRMS (MALDI-TOF) m/z: calcd, 852.4534 [M+2H_2O]; found, 852.5995 [M + 2H_2O].

Into 30 mL of DMF, 3 (163.3 mg, 0.2 mmol), 4 (214.4 mg, 0.6 mmol), DCC (136.2 mg, 0.66 mmol), and DMAP (80.6 mg, 0.66 mmol) were added and well dissolved. After adding 3 mL of triethylamine, the mixture was stirred at room temperature under N_2 for 48 h. The resulting mixture was then acidified by 10 mL of trifluoroacetic acid for 30 min, and then filtrated and precipitated in hexane three times to give the corresponding desired yellow solid compound, **5**, in 92% yield (mp 77.0 ± 1.1 °C). ^{1}H NMR (400 MHz, DMSO-d_6, δ): 8.45 (m, 2H, H of triazole), 8.05 (m, 2H, H of amide), 7.60 (m, 4H; H−Ar−triazole), 7.12−7.01 (m, 14H; H−Ar), 4.53 (s, 4H; CH_2−triazole), 3.83 (m, 4H; CH_2C−triazole), 3.57−3.13 (m, 20H; OCH_2), 3.02 (s, 20H; CH_2C≡
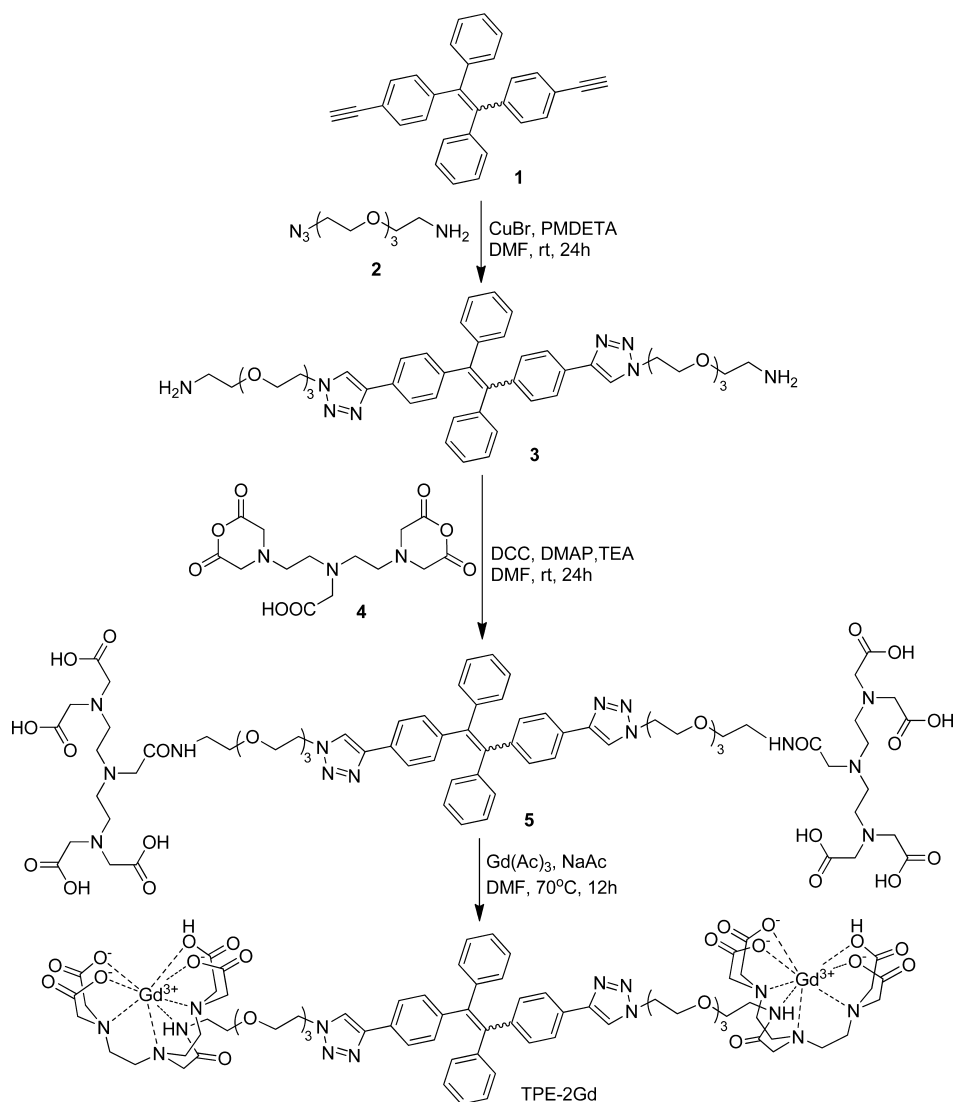
Figure 1. Synthetic route to dual-modal TPE-2Gd.

O), 2.90 (s, 20H; NCH$_2$); ^{13}C NMR (100 MHz, DMSO-d_6, δ): 172.6, 169.2, 145.9, 143.0, 142.6, 140.4, 131.3, 130.7, 129.0, 127.9, 126.7, 124.6, 121.8, 69.6, 68.6, 64.9, 55.1, 51.7, 49.6; IR (KBr): ν = 3437.2, 2954.9, 1726.3, 1635.6, 1460.1, 1396.4, 1226.7, 1089.8, 974.1, 908.5, 700.2 cm^{-1}; HRMS (MALDI-TOF) m/z: calcd, 1670.5896 [M − 4H + 3Na + K]; found, 1669.1871 [M − 4H + 3Na + K− H]; calcd, 1698.5795 [M − 6H + 6Na]; found, 1697.1949 [M − 6H + 6Na − H]; calcd, 1724.8194 [M − 5H + 2Na + 3K]; found, 1724.2223 [M − 5H + 2Na + 3K − H].

Then **5** (78.0 mg, 0.05 mmol), GdAc$_3$ (35.7 mg, 0.11 mmol), and NaAc (43.7 mg, 0.55 mmol) were dissolved into 20 mL of DMF. After stirring at 70 °C overnight, the resulting mixture was filtered and precipitated in hexane three times to give the desired yellow solid compound TPE-2Gd in 55% yield (mp 74.8 ± 1.6 °C). IR (KBr): ν = 3439.1, 1595.1, 1409.9, 1330.9, 1273.0, 1220.6, 1095.6, 933.5, 707.9, 653.9 cm^{-1}; HRMS (MALDI-TOF) m/z: calcd, 1984.5525 [M + 6H$_2$O]; found, 1984.4323 [M + 6H$_2$O].

2.4. Cell Culture and Imaging. HeLa cells were incubated in minimum essential medium (MEM), containing with 10% FBS, 100 U/ mL penicillin G, and 100 μg/mL streptomycin in a 5% CO$_2$, 90% relative humidity incubator at 37 °C. TPE-2Gd was dissolved in 1× PBS with the concentration of 10 mM as stock solution. For cell imaging, HeLa cells were seeded overnight on a coverslip mounted onto a 35 mm Petri dish and then stained with 30 μM TPE-2Gd for 4 h. The cells were rinsed three times with 1× PBS prior to imaging under the microscopes. For fixed cells, the cells were fixed with 75% ethanol solution for 30 min at 4

°C. The nuclei were stained with 10 μM PI for 15 min. After washing three times with 1× PBS, the cells were observed under the LSM7 DUO CLSM.

2.5. Cell Proliferation Assay. HeLa cells were seeded into a 96-well plate at a density of 8×10^3 cells per well overnight before treatment with TPE-2Gd in different concentrations. After 4 h incubation, the cells were washed three times with 1× PBS and fresh culture medium was added for additional 24 h incubation. The cell proliferation was measured using MTT assay according to the manufacturer's instructions. Briefly, the culture medium was replaced with 100 μL of freshly prepared MTT solution (0.5 mg/mL) in culture medium in each well. After incubation for 4 h, the MTT solution was gently removed and then 100 μL of DMSO was added into each well. After incubation at 37 °C for 10 min, the absorbance of individual wells at 490 nm was measured on a 1420 Victor Multi-Label Counter. All experiments were repeated three times.

2.6. In Vitro Relaxometry. The longitudinal relaxation rates ($1/T_1$) of TPE-2Gd and commercial contrast agent Magnevist in physiological saline at varying concentrations (0, 0.025, 0.2, 0.4, and 0.8 mM) of Gd^{3+} were recorded using 3.0 T Siemens Tim Trio MRI scanner equipped with a human head coil. Instrumental parameters were set as follows: pulse repetition time/echo time (TR/TE) = 400 ms/5.7 ms, field of view (FOV) = 225 × 225 mm^2, matrix size = 512 × 512 mm^2, slice thickness = 5 mm, at 25 °C.

2.7. In Vivo MR Imaging. All animal experiments were approved by the Animal Care and Use Committee of Tongji Medical College. Male SD rats (approximately 200 g, $n = 6$) were randomly assigned into two groups for TPE-2Gd and Magnevist imaging, respectively. The rats were anesthetized with 10% chloral hydrate at a dose of 3 mL/kg (ip). With rats in the prone position, MR imaging was performed at baseline (preinjection) and subsequent intervals after intravenous injection via caudal vein, at a dose of 0.1 mmol Gd^{3+}/kg body weight of the agent in 500 μL of physiological saline, using scan sequences with TR/TE = 5.15 ms/1.96 ms, FOV = 100×200 mm^2, matrix size =100×280 mm^2, slice thickness = 5 mm. MR images were then analyzed using Syngo fastView software (Siemens, Munich, Germany).

3. RESULTS AND DISCUSSION

3.1. Synthesis and Characterization of TPE-2Gd.
The synthetic route to TPE-2Gd is shown in Figure 1, and the detailed procedure is described in the Experimental Section. Briefly, 1,2-bis(4-ethynylphenyl)-1,2-diphenylethene (**1**)[20] and 2-{2-[2-(2-azidoethoxy)ethoxy]ethoxy}ethanamine (**2**)[21] were synthesized according to the literature. Click reaction of **1** and **2** via azide−alkyne cycloaddition catalyzed by Cu(I) yielded **3**, which was further modified with DTPA.[22] TPE-2Gd was obtained through the reaction between gadolinium acetate and **5**.[4−8] Compounds **3**, **5**, and TPE-2Gd were characterized by FT-IR, ^{1}H and ^{13}C NMR, and high-resolution MS (Figures S1−S4, Supporting Information).

The FT-IR spectrum of **1** shows strong C−H and C≡C stretching peaks at 3274 and 2105 cm^{-1}, respectively, while **2** has a characteristic -N$_3$ stretching band at 2115 cm^{-1} (Figure S1). These peaks disappear in the spectrum of **3**, indicative of the successful click reaction. In compound **5**, a new vibration band at 1722 cm^{-1} is observed, suggesting the functionalization of **3** with the DTPA ligands. Similar results are obtained from the ^{1}H and ^{13}C NMR spectra (Figure S2 and S3). The proton resonance peak of C≡C−H of **1** at 4.15 ppm disappears and a new peak at 8.41 ppm emerges upon formation of the triazole rings. Meanwhile, the proton resonance peaks adjacent to the azide group of **2** at 2.66 ppm disappear, while new peaks at 4.51 and 3.81 ppm occur for **3** (Figure S2). In the spectrum of **5**, proton resonance peaks at 8.06 ppm corresponding to CON−H appear owing to the amidation reaction. In ^{13}C NMR spectrum, the acetylene carbon atoms resonate at 76.8 and 83.1 ppm in **1**, which disappear completely in the spectrum of **3** (Figure S3). The emergence of new peaks in the aromatic region indicates the formation of the triazole rings, while the peak at 49.6 ppm is corresponding to the carbon next to the triazole ring. In the ^{13}C NMR spectrum of **5**, new peaks at 172.6, 169.2, 64.9, 55.1, and 51.6 ppm are recorded, which correspond to the COOH, CONH, C−HNC≡O, C−C≡O, and C−N from DTPA moieties, respectively, which confirm the successful linking of DTPA with TPE. Upon chelating Gd^{3+} with **5**, all proton and carbon resonances of TPE-2Gd disappear because of the strong relexation effect of Gd^{3+} ion. XPS spectrum shows that peaks 142.4, 285.0, 400.1, and 531.6 eV corresponding to Gd (4d), C (1s), N (1s), and O (1s) are visible in Figure S5, respectively. Quantitative analysis was calculated from the normalized areas of the Gd (4d), N (1s), and O (1s) peaks by using appropriate relative sensitivity factors (RSF$_{Gd}$ = 2.484, RSF$_N$ = 0.477 and RSF$_O$ = 0.780). The atomic ratio of Gd/N/O was found to be 0.052/0.324/0.624, consistent with theoretical calculation values (0.05/0.35/0.60).

3.2. AIE Properties of TPE-2Gd.
We then examined photophysical properties of TPE-2Gd. UV−vis spectrum shows a maximum absorption of TPE-2Gd is located at ~330

nm, which is similar to that of the parental fluorophores-TPE (Figure S6). When excited at 330 nm, TPE-2Gd is weakly fluorescent when the water fraction (f_w) in THF/water mixture is less than 50%. With the increase of f_w, the fluorescence of the solution is gradually enhanced and become highly emissive in pure aqueous solution, showing a typical AIE effect (Figure 2).
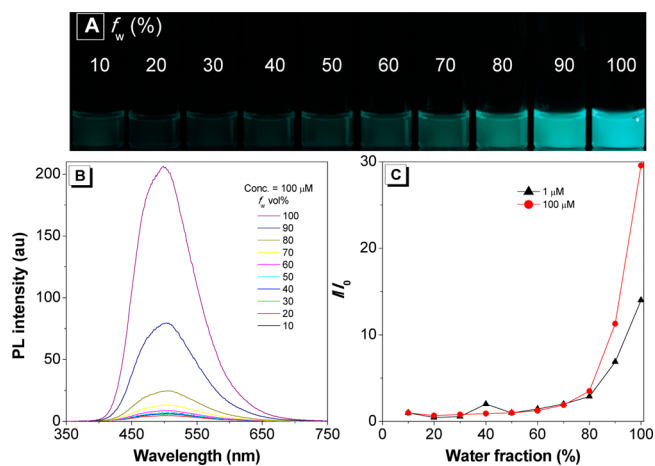

Figure 2. (A) Photographs taken under 365 nm UV irradiation and (B) emission spectra of TPE-2Gd in THF/H$_2$O mixtures with different water fractions (f_w). Concentration: 100 μM. Excitation wavelength: 330 nm. (C) Plot of relative PL intensity (I/I_0) versus the composition of the THF/H$_2$O mixtures of TPE-2Gd at different concentrations (1 and 100 μM).

The photograph in Figure 2A clearly shows the fluorescence enhancement of TPE-2Gd along with the increase of f_w in THF/water mixture. The solid-state quantum yield of TPE-2Gd is 15% measured with the integral-sphere technique.

From Figure 2C, we noticed that when the dye concentration is increased from 1 to 100 μM, the fluorescence of TPE-2Gd in pure water is increased by 1-fold. We speculated that the amphiphilic TPE-2Gd molecules may form micelles in high concentration. Thanks to the AIE property, the critical micelle concentration (CMC) of TPE-2Gd can be estimated using its fluorescence intensity (Figure 3). When the concentration is below the CMC, the dye molecules are well dissolved in solution and thus nonluminescent. The solution becomes emissive when the dye concentration is higher than 10 μM. Plotting the fluorescence intensity versus the dye concentration generates two lines, the intersection of which gives the CMC of 70 μM (Figure 3C). This value is much lower than that of sodium dodecyl sulfate (CMC = 8.2 mM),[23] mainly due to the strong hydrophobic interaction of the TPE moieties. The CMC value (50 μM, Figure S7) becomes even lower in PBS solution due to ionic strength effect. Owing to the amphiphilic nature of TPE-2Gd, numbers of TPE-2Gd molecules spontaneously come together and form TPE-2Gd nanoaggregates or micelles at concentrations above 70 μM in water and 50 μM in PBS solutions. Such low CMC ensures the formation of nano-aggregates in vivo even under dilution of bloodstream. The formation of nanoaggregates at high dye concentration is verified by means of transmission electron micrographs and zeta potential particle size analyzer (Figure 4). The effective diameter of the hydrated micelle is 164.9 nm, which shrinks to ~70 nm upon dehydration. The size of the nanoaggregates is appropriate both for in vitro cell uptake and in vivo circulation and biodistribution.[4−9]
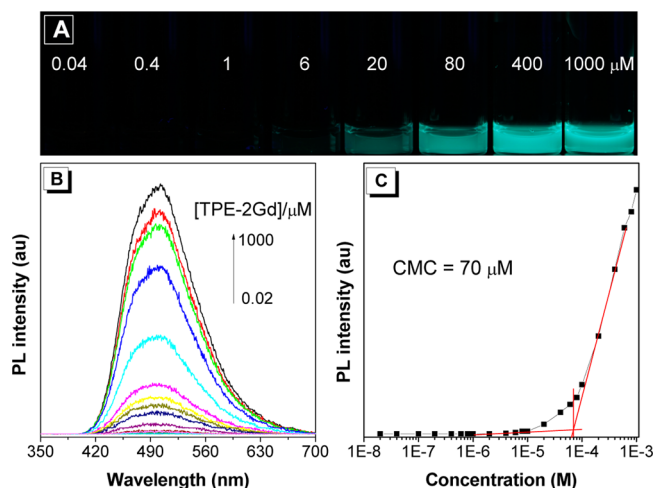
Figure 3. (A) Photographs taken under UV irradiation and (B) emission spectra of TPE-2Gd in aqueous solution at different concentrations. Excitation wavelength: 330 nm. (C) Plots of PL intensities versus concentrations of TPE-2Gd in water. The CMC of TPE-2Gd is 70 μM.
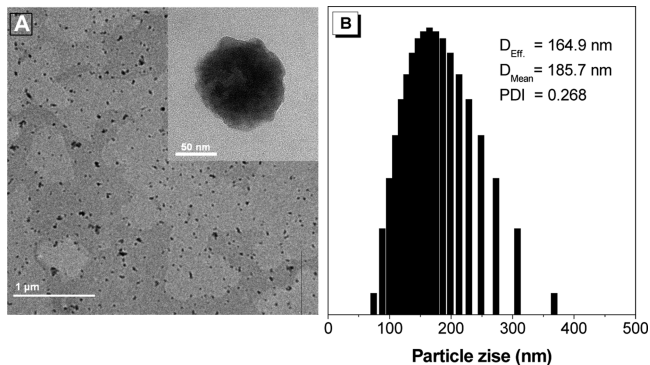

Figure 4. (A) Transmission electron micrographs and (B) particle size analysis of TPE-2Gd in water (100 μM).

3.3. In Vitro Fluorescent Imaging and Magnetic Relaxivity.

Magnevist, a common Gd-based MR contrast agent approved by the United States Food and Drug Administration, is a typical extracellular fluid agent which could rapidly circulate in extracellular regions or tissue space. TPE-2Gd, on the other hand, is capable of entering tumor cells, which is demonstrated by live cell imaging. HeLa cells were incubated with 30 μM TPE-2Gd for 4 h. TPE-2Gd can enter the cells and light up the cytoplasmic regions with blue fluorescence (Figure S8). To further confirm the staining region of TPE-2Gd, PI is used as a counterstain. PI is a nucleus dye that stains the nuclei of fixed cells. As shown in Figure 5, blue fluorescence surrounding the nuclei clearly indicates that TPE-2Gd selectively stains the cytoplasmic regions only. TPE-2Gd was internalized into living cells via the endocytosis pathway,[24] which enables TPE-2Gd to be used to track tumors at the cellular level, compensating to the tissue level by Magnevist.

The toxicity of TPE-2Gd was evaluated in HeLa cells using MTT assay. The cells were exposed to varying concentrations (0, 15, 30, 45, and 60 μM) of TPE-2Gd for 4 h and then incubated for 24 h in fresh culture medium for the assessment of internalization effect on cell proliferation. As depicted in Figure 6, TPE-2Gd is generally noncytotoxic when the concentration is lower than 30 μM; around 98.8% of the cells are viable upon the dye treatment. Even when the concentration is increased to 60
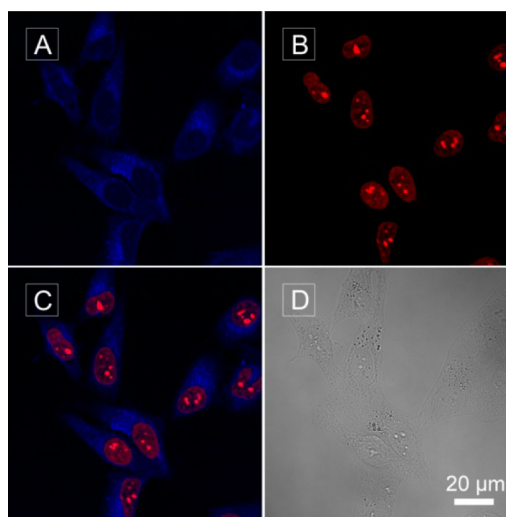

Figure 5. Fluorescence images of HeLa cells stained with (A) TPE-2Gd and then (B) PI. (C) Overlay of panels (A) and (B). (D) Bright-field images of the cells. [TPE-2Gd] = 30 μM.
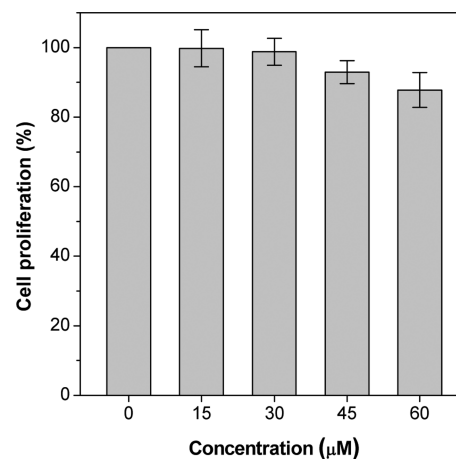

Figure 6. Cell proliferation of TPE-2Gd on HeLa cells evaluated by MTT assay. The cells were exposed to various concentrations of TPE-2Gd for 4 h and continued to grow for 24 h after replacement with fresh culture medium.

μM, which is two times higher than the working concentration in cell imaging experiments, the cell viability is still around 87.8%. This result indicates that TPE-2Gd is biocompatible for cell imaging and promising for further in vivo investigation.

On the other hand, to determine whether TPE-2Gd is an efficient MRI contrast agent, the longitudinal relaxation time or spin–lattice (T_1) of TPE-2Gd in aqueous solution was investigated as a function of Gd^{3+} concentration using 3.0 T MRI instrument at room temperature. As shown in Figure 7, the signal intensity (brightness) of mixture is enhanced with increased concentration of TPE-2Gd in buffer solution, similar to that of Magnevist at the same Gd^{3+} concentration. The longitudinal relaxivity (R_1), which refers to the paramagnetic component of the spin–lattice per unit concentration of the contrast agent, was determined to be 3.36 ± 0.10 mM$^{-1} \cdot$s^{-1} for TPE-2Gd and 3.70 ± 0.02 mM$^{-1} \cdot$s^{-1} for Magnevist (Figure 8).[11,12,25] TPE-2Gd possesses high relaxation rate comparable to Magnevist, suggesting TPE-2Gd can enhance the relaxation rate of water protons in its vicinity and lead to an increase of signal intensity.
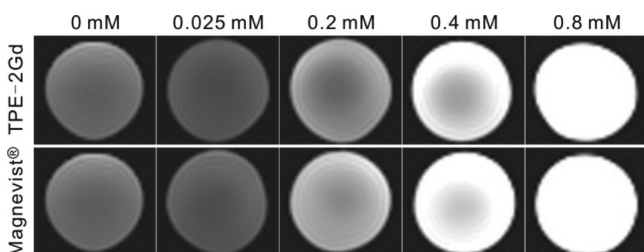
Figure 7. T_1-weighted MR images of TPE-2Gd and commercial contrast agent Magnevist at various concentration of Gd^{3+}. The samples are diluted with physiological saline.
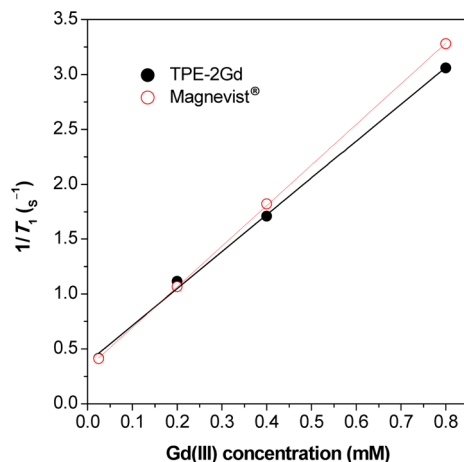

Figure 8. Water proton longitudinal relaxation rate $(1/T_1)$ of TPE-2Gd and Magnevist at various concentration of Gd^{3+}. According to the equation: $1/T_1 = 1/T_{1,0} + R_1[C_{Gd}]$. Relaxation rate: $R_{1,TPE-2Gd} = 3.36 \pm 0.10$ $mM^{-1} \cdot s^{-1}$; $R_{1,magnevist} = 3.70 \pm 0.02$ $mM^{-1} \cdot s^{-1}$.

**3.4. In Vivo MR Imaging.** In vivo MRI experiments were performed on live rats. Figure 9 shows dynamic coronal T_1-weighted MR images acquired in vivo before and after the intravenous injections of TPE-2Gd or Magnevist at a dose of 0.1 mmol Gd^{3+}/kg body weight. The signal intensity at baseline (before injection) was recorded for comparison with that of postcontrast enhancement. The regions of interest (ROIs) were delineated in the heart, liver, and bladder with different style lines as shown in Figure 9. All circulating blood is rhythmically pumped to each organ by the heart; therefore, the signal intensity of blood flow in cardiac chambers can reflect the residual quantity of Gd^{3+}. At baseline (before injection), cardiac chambers are hypointense. The cardiocoelomic contrast enhancement is observed in the first image after injection of TPE-2Gd or Magnevist (1 min). However, the hyperintense signal of Magnevist is rapidly decreased (<5 min) because of its high glomerular filtration rate, whereas for TPE-2Gd administration the signal still remains much brighter than that of baseline. As shown in Figure 10A, upon injection of the contrast agent, the signal intensity in heart returned to the level of baseline within 60 min for Magnevist, while TPE-2Gd can still maintain 42% of the initial signal even after 150 min. The in vivo T_1-weighted MR imaging also shows that TPE-2Gd has an intravascular half-life up to 60 min, which is much longer than that of Magnevist (about 10 min). This result demonstrates the long circulation lifetime of TPE-2Gd in blood, which can be attributed to the low filtration rate of the large nanoaggregates via glomerular filtration membrane.

Another organ in which we were interested is the liver. Liver is a vital organ involved in blood supply. Many species of occupying lesions are derived from liver cells and metastasized to other organs, such as focal nodular hyperplasia (FNH), hepatic hemangioma, adenoma, hepatocellular carcinoma (HCC), liver metastasis of colon cancer, and so forth. Thus, liver specific contrast imaging is of great importance for distinguishing between lesion and normal tissues. Similar to that in heart, the intensity in liver is enhanced upon Magnevist injection and decreases rapidly to the baseline within 60 min. In contrast, the signal from TPE-2Gd remains hyperintense in comparison with
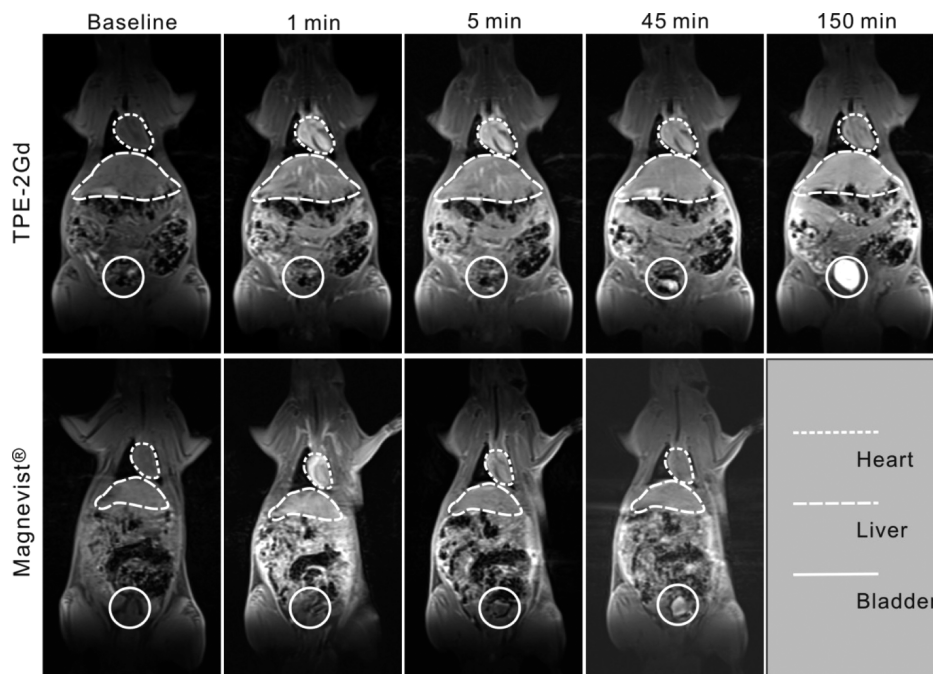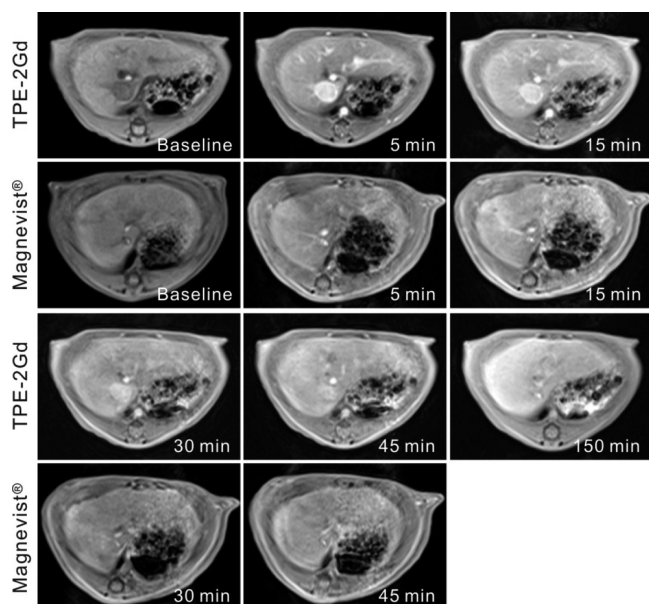

Figure 9. Coronal T_1-weighted MR images of rat after intravenous injection of TPE-2Gd and Magnevist with concentration of 0.1 mmol/kg Gd^{3+}.
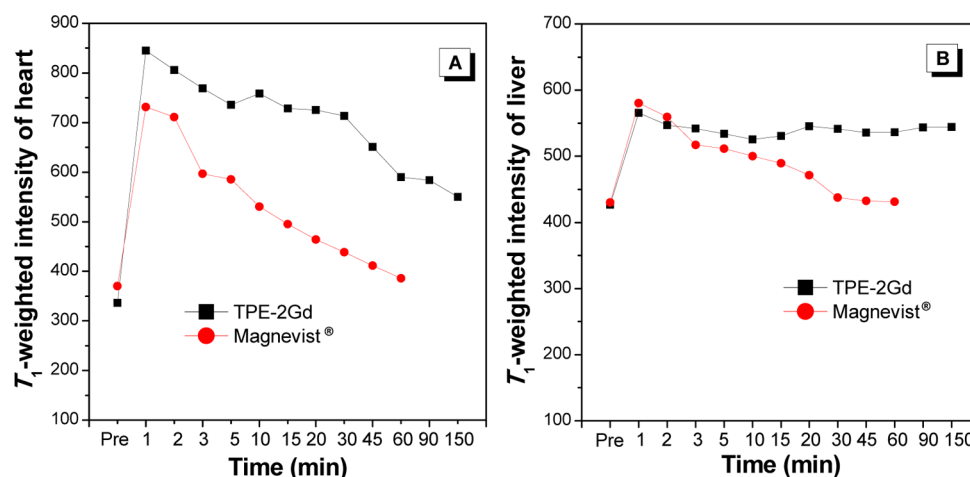
Figure 10. Quantitative analysis of T_1-weighted image of (A) heart and (B) liver.

baseline, up to 150 min after TPE-2Gd administration (Figure 9). Meanwhile, axial images could exhibit the anatomical structure and enhancement effect of liver in detail (Figure 11).

Figure 11. Axial T_1-weighted MR images through the liver of rat after intravenous injection of TPE-2Gd and Magnevist with concentration of 0.1 mmol/kg Gd^{3+}.

During the early phase of TPE-2Gd administration, the aorta, inferior vena cava, and intrahepatic vena cava possess higher intensity over the peripheral tissue; the signal intensity from the liver parenchyma is increased gradually after injection. However, after Magnevist administration, the enhancement of the MRI signal in liver is not as remarkable as that of TPE-2Gd. The longer circulation time and the higher contrast achieved by TPE-2Gd can be ascribed to its ability to form nanoaggregates and to enter the intracellular regions.

Quantitative analysis of the signal intensity in the liver demonstrates that the intensity after administration of the contrast agent increases to the maximum within 1 min and then decreases gradually. Interestingly, for TPE-2Gd, the intensity decreases by ~20% in the first 20 min after injection and then increases by ~10% afterward (Figure 10B); for Magnevist, after

reaching the maximum in 1 min, the intensity just decreases monotonically. Because TPE-2Gd molecules form nanoaggregates in bloodstream, they could be trapped specifically and predominantly in the macrophages of a reticuloendothelial system (RES).[26] Kupffer cells, locating in the liver, are specialized macrophages as an integral part of the sinusoids. The Kupffer cells remove TPE-2Gd from bloodstream through phagocytosis pathway, resulting in the accumulation of TPE-2Gd nanoaggregates in the liver tissue. Therefore, the signal intensity in liver is re-enhanced after 20 min of injection and kept at a high level above the baseline. Based on this hypothesis, TPE-2Gd could be used to discriminate lesion and normal tissue. Since hepatic metastases lack Kupffer cells, they would not show any contrast-enhancement after TPE-2Gd administration. On the other hand, focal liver lesions with Kupffer cells such as FNH, adenoma, and well-differentiated HCC would exhibit a significant enhancement in signal intensity on T_1-weighted images, which can reveal the uptake and accumulation of the nanoaggregates.

In vivo elimination is an important parameter for animal experiments and preclinical applications. Magnevist is rapidly eliminated from body into urine, which is illustrated by the hyperintense signal in the bladder at 5 min after injection. The images shown in Figure 9 show that TPE-2Gd can also be excreted through kidney and accumulated in the bladder at 150 min after injection. The foregoing analysis indicates TPE-2Gd exhibits prolonged circulation time of Gd^{3+} in blood owing to the formation of nanoaggregates. These nanoaggregates can be disassembled into smaller particles or individual molecules slowly and then be eliminated via the kidney.[27] All the results indicate that TPE-2Gd is a promising T_1-weighted contrast agent for liver specific imaging.

4. CONCLUSION

In summary, we have designed and synthesized a remarkable dual-modal fluorescent-MRI contrast agent, TPE-2Gd, as positive blood pool and liver specific MRI contrast agents. The amphiphilic TPE-2Gd molecules can form nanoscaled micelles in aqueous solution. These nanoaggregates are highly emissive, showing a typical AIE effect. With excellent photostability and biocompatibility, TPE-2Gd is well suited for use as a fluorescent agent for live cell imaging. As a MRI contrast agent, TPE-2Gd possesses comparable magnetic relaxivity as the commercial Gd-based MRI contrast agent Magnevist. The in vivo MRI imaging

10789

dx.doi.org/10.1021/am502282f | ACS Appl. Mater. Interfaces 2014, 6, 10783−10791

of live rats demonstrates the long circulation time and good body elimination of TPE-2Gd, owing to the formation and dissociation of the nanoaggregates of TPE-2Gd, respectively. The specificity to the liver also implies TPE-2Gd could be used to discriminate lesion and normal tissues. This work represents new generation of materials which combine the AIE property and magnetic relaxivity to generate a dual-modal, MRI and fluorescent agent for clinical diagnosis. The synthesis of red AIE emitters conjugated to DTPA-Gd is ongoing in our laboratory to enhance in vivo both MRI and fluorescent imaging.

■ ASSOCIATED CONTENT

Ⓢ Supporting Information

FTIR, ^{1}H NMR and ^{13}C NMR spectra of compounds **1**, **2**, **3**, **5** and TPE-2Gd. XPS spectrum of TPE-2Gd. UV spectrum of TPE-2Gd in aqueous solution. PL spectra of TPE-2Gd in PBS solution at different concentrations. Fluorescent image of live HeLa cells stained with TPE-2Gd. This material is available free of charge via the Internet at http://pubs.acs.org.

■ AUTHOR INFORMATION

Corresponding Authors

*E-mail: qc_zheng@mail.hust.edu.cn.
*E-mail: tangbenz@ust.hk.

Author Contributions

[1]Y.C. and M.L. contributed equally to this work.

Notes

The authors declare no competing financial interest.

■ ACKNOWLEDGMENTS

■ REFERENCES

(1) Schima, W.; Mukerjee, A.; Saini, S. Contrast-Enhanced MR Imaging. *Clin. Radiol.* **1996**, *51*, 235−244.

(2) Caravan, P. Strategies for Increasing the Sensitivity of Gadolinium Based MRI Contrast Agents. *Chem. Soc. Rev.* **2006**, *35*, 512−523.

(3) Villaraza, A. J. L.; Bumb, A.; Brechbiel, M. W. Macromolecules, Dendrimers, and Nanomaterials in Magnetic Resonance Imaging: The Interplay between Size, Function, and Pharmacokinetics. *Chem. Rev.* **2010**, *110*, 2921−2959.

(4) Tang, J.; Sheng, Y.; Hu, H.; Shen, Y. Macromolecular MRI Contrast Agents: Structures, Properties and Applications. *Prog. Polym. Sci.* **2013**, *38*, 462−502.

(5) Bryson, J. M.; Reineke, J. W.; Reineke, T. M. Macromolecular Imaging Agents Containing Lanthanides: Can Conceptual Promise Lead to Clinical Potential? *Macromolecules* **2012**, *45*, 8939−8952.

(6) Boase, N. R. B.; Blakey, I.; Thurecht, K. J. Molecular Imaging with Polymers. *Polym. Chem.* **2012**, *3*, 1384.

(7) Thurecht, K. J. Polymers as Probes for Multimodal Imaging with MRI. *Macromol. Chem. Phys.* **2012**, *213*, 2567−2572.

(8) Zhang, B.; Jin, H.; Li, Y.; Chen, B.; Liu, S.; Shi, D. Bioinspired Synthesis of Gadolinium-Based Hybrid Nanoparticles as MRI Blood Pool Contrast Agents with High Relaxivity. *J. Mater. Chem.* **2012**, *22*, 14494−14501.

(9) Matsumura, Y.; Maeda, H. A New Concept for Macromolecular Therapeutics in Cancer Chemotherapy: Mechanism of Tumoritropic Accumulation of Proteins and the Antitumor Agent Smancs. *Cancer Res.* **1986**, *46*, 6387−6392.

(10) Frullano, L.; Meade, T. J. Multimodal MRI Contrast Agents. *J. Biol. Inorg. Chem.* **2007**, *12*, 939−949.

(11) Li, K.; Ding, D.; Huo, D.; Pu, K. Y.; Thao, N. N. P.; Hu, Y.; Li, Z.; Liu, B. Conjugated Polymer Based Nanoparticles as Dual-Modal Probes for Targeted In Vivo Fluorescence and Magnetic Resonance Imaging. *Adv. Funct. Mater.* **2012**, *22*, 3107−3115.

(12) Ding, D.; Wang, G.; Liu, J.; Li, K.; Pu, K. Y.; Hu, Y.; Ng, J. C. Y.; Tang, B. Z.; Liu, B. Hyperbranched Conjugated Polyelectrolyte for Dual-modality Fluorescence and Magnetic Resonance Cancer Imaging. *Small* **2012**, *8*, 3523−3530.

(13) Hüber, M. M.; Staubli, A. B.; Kustedjo, K.; Gray, M. H. B.; Shih, J.; Fraser, S. E.; Jacobs, R. E.; Meade, T. J. Fluorescently Detectable Magnetic Resonance Imaging Agents. *Bioconjugate Chem.* **1998**, *9*, 242−249.

(14) Li, H.; Gray, B. D.; Corbin, I.; Lebherz, C.; Choi, H.; Lund-Katz, S.; Wilson, J. M.; Glickson, J. D.; Zhou, R. MR and Fluorescent Imaging of Low-Density Lipoprotein Receptors. *Acad. Radiol.* **2004**, *11*, 1251−1259.

(15) Manning, H. C.; Goebel, T.; Thompson, R. C.; Price, R. R.; Lee, H.; Bornhop, D. J. Targeted Molecular Imaging Agents for Cellular-Scale Bimodal Imaging. *Bioconjugate Chem.* **2004**, *15*, 1488−1495.

(16) Luo, J.; Xie, Z.; Lam, J. W. Y.; Cheng, L.; Chen, H.; Qiu, C.; Kwok, H. S.; Zhan, X.; Liu, Y.; Zhu, D.; Tang, B. Z. Aggregation-Induced Emission of 1-Methyl-1,2,3,4,5-Pentaphenylsilole. *Chem. Commun.* **2001**, *18*, 1740−1741.

(17) Hong, Y.; Lam, J. W. Y.; Tang, B. Z. Aggregation-Induced Emission: Phenomenon, Mechanism and Applications. *Chem. Commun.* **2009**, 4332−4353.

(18) Hong, Y.; Lam, J. W. Y.; Tang, B. Z. Aggregation-Induced Emission. *Chem. Soc. Rev.* **2011**, *40*, 5361−5388.

(19) Ding, D.; Li, K.; Liu, B.; Tang, B. Z. Bioprobes Based on AIE Fluorogens. *Acc. Chem. Res.* **2013**, *46*, 2441−2453.

(20) Hu, R. R.; Maldonado, J. L.; Rodriguez, M.; Deng, C. M.; Jim, C. K. W.; Lam, J. W. Y.; Yuen, M. M. F.; Ramos-Ortiz, G.; Tang, B. Z. Luminogenic Materials Constructed from Tetraphenylethene Building Blocks: Synthesis, Aggregation-Induced Emission, Two-Photon Absorption, Light Refraction, and Explosive Detection. *J. Mater. Chem.* **2012**, *22*, 232−240.

(21) Goswami, L. N.; Houston, Z. H.; Sarma, S. J.; Jalisatgi, S. S.; Hawthorne, M. F. Efficient Synthesis of Diverse Heterobifunctionalized Clickable Oligo(Ethylene Glycol) Linkers: Potential Applications in Bioconjugation and Targeted Drug Delivery. *Org. Biomol. Chem.* **2013**, *11*, 1116−1126.

(22) Ardestani, M. S.; Arabzadeh, A. J.; Heidari, Z.; Hosseinzadeh, A.; Ebrahimi, H.; Hashemi, E.; Mosayebnia, M.; Shafiee-Alavidjeh, M.; Alavi, A.; Babaei, M. H.; Rahmim, A.; Ebrahimi, S. E. S.; Amanlou, M. Novel and Facile Methods for the Synthesis of DTPA-Mono-Amide: a New Completely Revised Strategy in Radiopharmaceutical Chemistry. *J. Radioanal. Nucl. Chem.* **2010**, *283*, 447−455.

(23) Mukerjee, P.; Mysels, K. J. *Critical Micelle Concentration of Aqueous Surfactant Systems*, NSRDS-NBS 36; U.S. Government Printing Office: Washington, DC, 1971.

(24) Li, M.; Hong, Y.; Wang, Z. K.; Chen, S. J.; Gao, M.; Kwok, R. T. K.; Qin, W.; Lam, J. W. Y.; Zheng, Q. C.; Tang, B. Z. Fabrication of Chitosan Nanoparticles with Aggregation-Induced Emission Characteristics and Their Applications in Long-Term Live Cell Imaging. *Macromol. Rapid Commun.* **2013**, *34*, 767−771.

(25) Cheung, E. N. M.; Alvares, R. D. A.; Oakden, W.; Chaudhary, R.; Hill, M. L.; Pichaandi, J.; Mo, G. C. H.; Yip, C.; Macdonald, P. M.; Stanisz, G. J.; van Veggel, F. C. J. M.; Prosser, R. S. Polymer-Stabilized Lanthanide Fluoride Nanoparticle Aggregates as Contrast Agents for Magnetic Resonance Imaging and Computed Tomography. *Chem. Mater.* **2010**, *22*, 4728−4739.

(26) Ba-Ssalamah, A.; Uffmann, M.; Saini, S.; Bastati, N.; Herold, C.; Schima, W. Clinical Value of MRI Liver-Specific Contrast Agents: a Tailored Examination for a Confident Non-Invasive Diagnosis of Focal Liver Lesions. *Eur. Radiol.* **2009**, *19*, 342−357.

(27) Zhang, B.; Li, Q.; Yin, P.; Rui, Y.; Qiu, Y.; Wang, Y.; Shi, D. Ultrasound-Triggered BSA/SPION Hybrid Nanoclusters for Liver-Specific Magnetic Resonance Imaging. *ACS Appl. Mater. Interfaces* **2012**, *4*, 6479−6486.